www.acsmaterialsletters.org

# Petrified Hollow Fiber Membranes with **Hierarchical Pores**

Lu Liu, Ching-En Ku, and Chen Zhang\*



Downloaded via UNIV OF MARYLAND COLG PARK on May 2, 2022 at 17:37:00 (UTC). See https://pubs.acs.org/sharingguidelines for options on how to legitimately share published articles.

Cite This: ACS Materials Lett. 2022, 4, 938-943



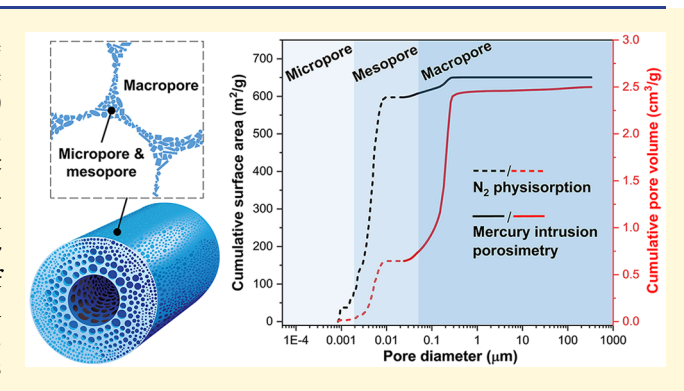
**ACCESS** 

Metrics & More

Article Recommendations

Supporting Information

ABSTRACT: Porous oxide hollow fiber membranes are broadly useful for filtration and chemical separation. They are traditionally formed by phase inversion-sintering above 1200 °C, which is expensive limiting their large-scale applications. Inspired by the natural wood petrification process, we report fabrication of porous oxide hollow fiber membranes via petrification of polymer hollow fiber templates at a much lower temperature (600 °C). These novel petrified hollow fiber membranes reproduce the asymmetric macropore structure of their polymer hollow fiber templates, thereby allowing rejection of macromolecular solutes without a secondary coating layer. They have a unique hierarchical micro-/meso-/macroporous structure with simultaneous high surface area and large pore



volume. The findings of this work pave the way for wider applications of porous oxide membranes. More broadly, they allow simple and inexpensive control of the geometry of hierarchically porous oxides.

orous oxides (e.g., silica, metal oxides) are broadly used as membranes<sup>1,2</sup> and adsorbents<sup>3</sup> for chemical separations. While tunable surface area and pore volume are crucial to provide attractive transport and adsorption properties, controlling the geometry of porous oxide membranes and adsorbents is often important for large-scale applications. For example, hollow fiber is the industry-preferred geometry for porous oxide membranes, which can be used as pressure-driven filtration membranes<sup>4</sup> or supports of thin molecularly selective membranes (e.g., zeolite membranes, 2,5,6 ion-transport perovskite membranes). Compared with polymer hollow fibers, oxide hollow fibers are more thermally stable and chemically resistant. Unlike most porous polymer hollow fibers that can be inexpensively solution-processed at room temperature,8 porous oxide hollow fibers are traditionally made by expensive phase inversion-sintering,<sup>9</sup> tape casting-sintering,<sup>10</sup> or melt processing, 11 which often occur above 1200–1500 °C. Notably, phase inversion-sintering 12 relies on sintering of polymer hollow fibers consisting of preformed nonporous oxide (e.g.,  $\alpha$ -alumina) particles. Porous oxide hollow fibers made by phase inversion-sintering can be abundant in macropores, however, often have few mesopores and micropores and low surface area. A number of soft-templating and hard-templating approaches <sup>13–16</sup> were developed to fabricate hierarchically porous oxides with tunable surface area and pore volume; however, none have been able to form porous oxide hollow fibers suitable for separation applications. There is

significant value to develop novel methods that can inexpensively fabricate porous oxide hollow fibers while providing both tunable surface area and pore volume.

Inspired by petrified wood,<sup>17</sup> we developed an innovative petrification method to fabricate porous oxide hollow fiber membranes at moderate temperatures using macroporous polymer hollow fibers as templates. These novel porous oxide membranes, which we name "petrified hollow fiber membranes", have hierarchical pores with simultaneous high surface area and large pore volume. Wood petrification occurs in nature by exchange of wood organic cell tissues with surrounding siliceous precursors, which forms silica monoliths preserving both the macroscopic geometry and microscopic cell structure of the wood templates. Asymmetric macroporous P84 polyimide hollow fibers (Figure 1a) were fabricated by dry-jet/wet-quench spinning and used as polymer hollow fiber templates. 18 To imitate wood petrification, the polymer hollow fiber templates were soaked in a siliceous precursor (vinyltrimethoxysilane) followed by exposure to water vapor at room temperature, 19 which provided treated polymer hollow fiber

Received: January 23, 2022 Accepted: April 7, 2022 Published: April 11, 2022





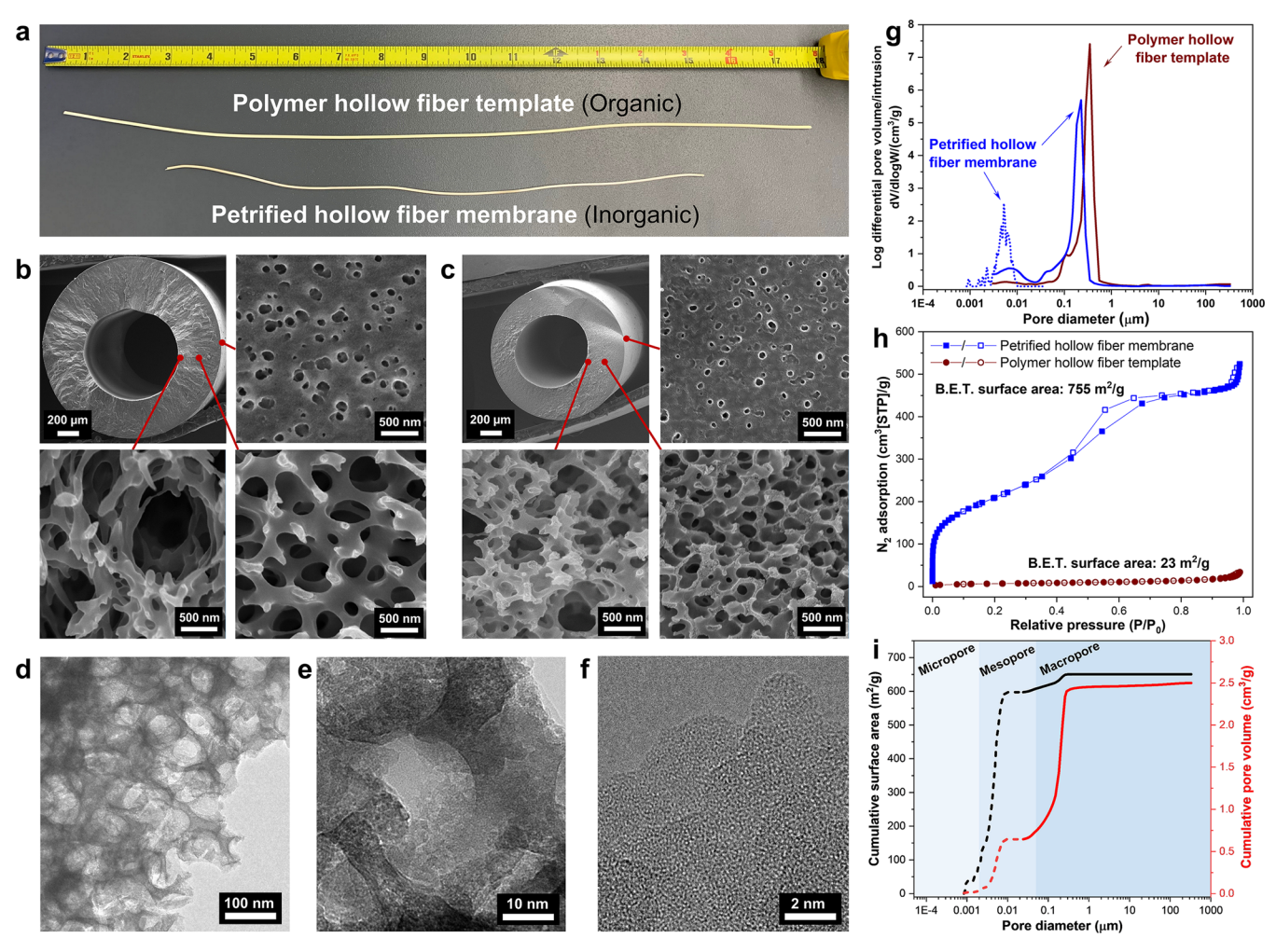


Figure 1. The hierarchical micro-/meso-/macroporous structure of petrified hollow fiber membranes. (a) Photo showing a polymer hollow fiber template (top) and a petrified hollow fiber membrane (bottom). The tape measure (unit given in inch) is shown to indicate the fiber length. (b) SEM images showing the morphology and pore structure of polymer hollow fiber templates. (c) SEM images showing the morphology and pore structure of petrified hollow fiber membranes. TEM images showing (d) macropore structure of petrified hollow fiber membranes, (e) macropore wall consisting of aggregated nanoparticles, and (f) nonporous nanoparticles inside the macropore wall. (g) Pore size distribution measured by mercury intrusion porosimetry (solid lines). The micropore–mesopore size distribution (dashed line) obtained by NLDFT (from  $N_2$  physisorption) is also shown for the petrified hollow fiber membranes. (h)  $N_2$  physisorption isotherms at 77 K. The adsorption branch is shown by solid symbols. The desorption branch is shown by hollow symbols. (i) Merged cumulative surface area and cumulative pore volume of petrified hollow fiber membranes. The dashed lines represent data obtained by NLDFT (from  $N_2$  physisorption). The solid lines represent data obtained from mercury intrusion porosimetry.

templates. While wood petrification usually takes thousands or millions of years in nature, the treated polymer hollow fiber templates were heated in air at 600 °C to accelerate polymer template decomposition. After air heating for 2 h, white-colored petrified hollow fiber membranes (Figure 1a) were formed preserving the geometry of the yellow-colored polymer hollow fiber templates. The hollow fiber length and diameter both shrunk by ~30% following air heating. Energy dispersive X-ray analysis (EDX, Figure S1) suggests the petrified hollow fiber membranes are fully inorganic comprising silicon and oxygen. Thermogravimetric analysis (TGA, Figure S2) shows ~23% weight of the treated polymer hollow fiber template was retained following air heating at 600 °C. According to X-ray diffraction (XRD, Figure S3), the petrified hollow fiber membranes consist of amorphous silica.

Like wood cell structure is preserved in petrified wood, the macropore structure of polymer hollow fiber templates (Figure 1b) was preserved in the petrified hollow fiber membranes

(Figure 1c) with remarkable resemblance. Scanning electron microscopy (SEM) suggests both the polymer hollow fiber template and petrified hollow fiber membrane have asymmetric pore morphology, i.e., pore size gradient is seen in the hollow fiber radial direction with smaller pores at the hollow fiber top surface and larger pores at the hollow fiber bore side. Also, the hollow fiber pore size was reduced following petrification. The polymer hollow fiber template had top surface pore diameter ~84 nm (Figure 1b), while the petrified hollow fiber membrane had top surface pore diameter ~49 nm (Figure 1c). Remarkably, even the slight eccentricity of the polymer hollow fiber template was reproduced in the petrified hollow fiber membranes. Transmission electron microscopy (TEM) indicates the macropore walls (Figure 1d) of petrified hollow fiber membranes consist of randomly aggregated nanoparticles (Figure 1e), which appear to be nonporous under highresolution TEM (Figure 1f).

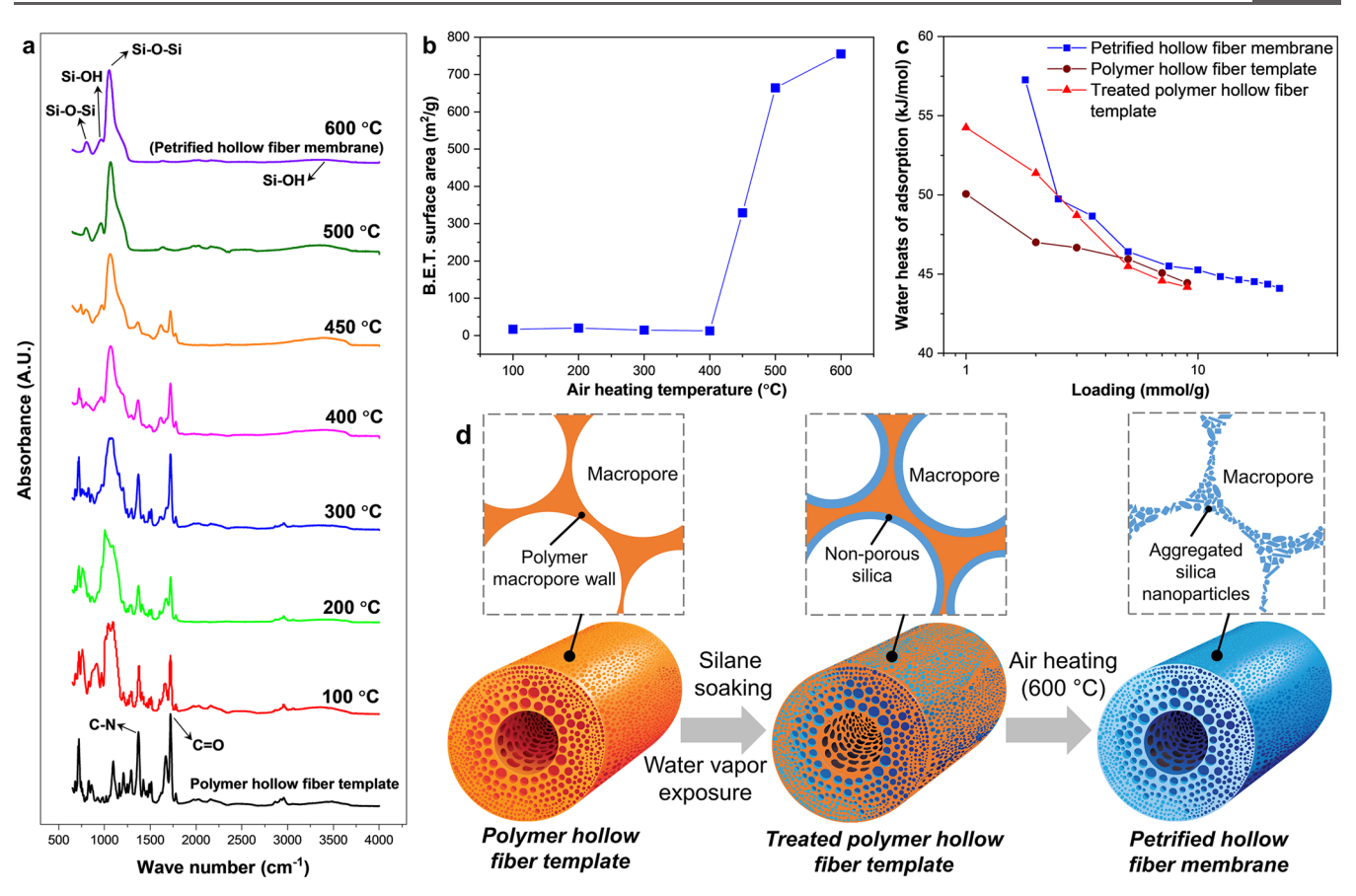


Figure 2. Elucidating the formation mechanism of petrified hollow fiber membranes. (a) FT-IR spectra showing the effects of air heating temperature on the chemical structure of treated polymer hollow fiber templates. The FT-IR spectra of the bare polymer hollow fiber template are shown for reference. (b) The effects of air heating temperature on B.E.T. surface area of treated polymer hollow fiber template. (c) Water isosteric heats of adsorption of polymer hollow fiber templates (burgundy circles), treated polymer hollow fiber templates (red triangles), and petrified hollow fiber membranes (blue squares). (d) Schematics illustrating the hypothetical formation mechanism of petrified hollow fiber membranes.

Mercury intrusion porosimetry (MIP, Figure 1g) suggests the pore structure of polymer hollow fiber templates was dominated by macropores (d > 50 nm), whereas both macropores and mesopores (2 nm < d < 50 nm) were seen in petrified hollow fiber membranes. In agreement with SEM, MIP indicates the macropore structure of the polymer hollow fiber templates was reproduced in the petrified hollow fiber membranes with almost identical shape of macropore size distribution curves. The petrified hollow fiber membranes have higher porosity (79.9 vs 75.2%), skeletal density (1.8 vs 1.3 g/cm³), and tortuosity (4.1 vs 3.1) than the polymer hollow fiber templates (Table S1).

Nitrogen physisorption (77 K) shows that the polymer hollow fiber templates have a low Brunauer–Emmett–Teller (B.E.T.) surface area (23 m²/g) and the Type II N₂ physisorption isotherm (Figure 1h and Figure S4) typical for macroporous materials. The petrified hollow fiber membranes have the Type IV isotherm and a considerably higher B.E.T. surface area (755 m²/g). Analysis of the N₂ physisorption isotherm by the non-local density functional theory (NLDFT, Figure 1g) suggests the petrified hollow fiber membranes comprise a small amount of micropores (d < 2 nm). Thus, the petrified hollow fiber membranes have a unique hierarchical micro-/meso-/macroporous structure. In addition to nitrogen physisorption (77 K), argon physisorption (87 K) was carried out on the petrified hollow fiber membranes. The

results of argon physisorption agree with nitrogen physisorption in that the petrified hollow fiber membranes consist of both micropores and mesopores (Figure S4). According to TEM (Figure 1e), the micropores and mesopores were possibly provided by the space between aggregated nonporous nanoparticles inside the macropore walls.

It is worthwhile to note that MIP underestimates the amount of mesopores in petrified hollow fiber membranes (Figure 1g). Hence, the cumulative surface area and pore volume curves obtained by NLDFT (Figure S5) and MIP (Figure S6) were merged (Figure 1i and Table S2) to provide the NLDFT-MIP surface area (651 m<sup>2</sup>/g) and NLDFT-MIP pore volume (2.5 cm<sup>3</sup>/g). The hierarchical micro-/meso-/ macroporous structure of petrified hollow fiber membranes gives simultaneous high surface area and large pore volume. While the high surface area is attributed to the mesopores, the macropores are responsible for the large pore volume. Consisting of only three steps of silane soaking, moisture exposure, and air heating, the novel petrification method provides a simple and catalyst-free route to fabricate hierarchical micro-/meso-/macroporous oxides with high surface area and large pore volume.

To elucidate the formation mechanism of petrified hollow fiber membranes, the treated polymer hollow fiber templates were air heated to  $100-600~^{\circ}\text{C}$  and characterized by Fourier-transform infrared spectroscopy (FT-IR, Figure 2a) and  $N_2$ 

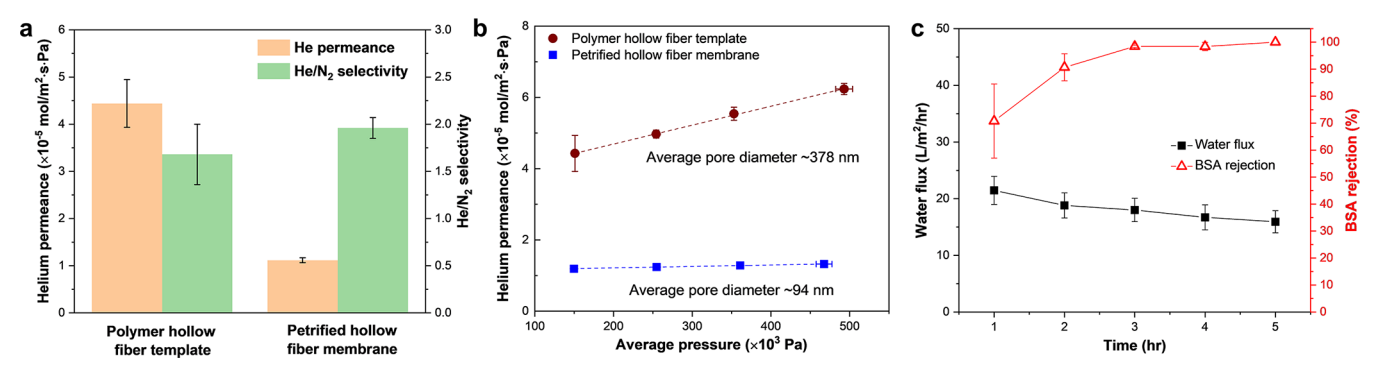


Figure 3. Transport properties of petrified hollow fiber membranes. (a) Helium and nitrogen permeation results of petrified hollow fiber membranes and polymer hollow fiber templates. (b) Determination of hollow fiber average pore diameters by helium permeation (Supporting Information). (c) Water flux and rejection of petrified hollow fiber membranes under cross-flow filtration test of a BSA solution (0.5 g/L).

physisorption (Figure 2b and Figure S7). As the air heating temperature increased, the fibers became darker (Figure S8) possibly due to polymer template decomposition, which is evidenced by progressively weaker polyimide peaks in the IR spectra. As the temperature reached 600 °C, the fibers became white and the IR spectra showed well-defined silica peaks<sup>21</sup> with all polyimide peaks<sup>22</sup> disappeared. The B.E.T. surface area stayed under  $30 \text{ m}^2/\text{g}$  as the air heating temperature was below 450 °C and dramatically increased as the temperature was raised to above 450 °C. The increase in surface area was due to enhanced microporosity and mesoporosity, with mesoporosity becoming more dominant as the temperature reached 600 °C (Figure S9). It is worthwhile to note this temperature overlaps with the decomposition temperature of the P84 polyimide (~400–450 °C, Figure S2). Water vapor sorption (Figure 2c and Figure S10) was used to determine water isosteric heats of adsorption using the Clausius-Clapeyron equation.<sup>23</sup> The treated polymer hollow fiber templates showed isosteric heats of adsorption higher than the bare polymer hollow fiber templates and lower than the petrified hollow fiber membranes.

The hypothetical formation mechanism of petrified hollow fiber membranes is illustrated in Figure 2d. Silane molecules are first infiltrated into the macropore space of polymer hollow fiber templates during soaking. Following exposure to water vapor, silane hydrolysis and condensation occur in the macropores of polymer hollow fiber templates forming silica. The silica formation is evidenced by increased water isosteric heat of adsorption (Figure 2c) and the appearance of the Si-O-Si peak in the IR spectra (Figure 2a). As the surface area remains low (Figure 2b), the silica is likely nonporous. As the temperature is increased to 400-450 °C, rapid weight loss of the polymer hollow fiber template occurs, causing the formation of silica nanoparticles and an increased surface area. As the temperature further increases, the silica nanoparticles fill in the space left by the progressively removed polymer template. The space-filling is possibly accompanied by continuing hydrolysis and condensation reactions at the interfaces of neighboring silica nanoparticles, which is assisted by water vapor produced as a result of polymer template decomposition.<sup>24</sup> The continuing hydrolysis and condensation are evidenced by strengthening of the Si-O-Si peak in the IR spectra. The space-filling allows the petrified hollow fiber membranes to reproduce both the geometry and macropore structure of the removed polymer hollow fiber template.

Single-component helium and nitrogen permeation was carried out at room temperature (Figure 3a). The polymer hollow fiber templates were highly permeable with helium permeance  $\sim 4.4 \times 10^{-5} \text{ mol/m}^2 \cdot \text{s} \cdot \text{Pa}$  and helium/nitrogen selectivity ~1.7. The petrified hollow fiber membranes showed lower helium permeance (~1.1 × 10<sup>-5</sup> mol/m<sup>2</sup>·s·Pa) and negligible change in helium/nitrogen selectivity. Notably, the petrified hollow fiber membranes remained highly permeable and hence are attractive as supports for molecularly selective inorganic membranes. The lower helium permeance of petrified hollow fiber membranes can be attributed to smaller macropores. While micropores and mesopores were found in petrified hollow fiber membranes, they do not form a continuous barrier. Hence, molecular transport in petrified hollow fiber membranes is dominated by the interconnected macropores. By varying the transmembrane pressure (TMP) of helium permeation, the hollow fiber average pore diameters were determined (Figure 3b) by deconvoluting the contributions of Knudsen diffusion and viscous flow (Supporting Information).<sup>25</sup> The results suggest the polymer hollow fiber templates have larger average pore diameter (378 nm) than the petrified hollow fiber membranes (94 nm), which is consistent with the trend observed by MIP (Figure 1g). Notably, the permeances increased linearly with TMP up to 7 bar, suggesting petrified hollow fiber membranes are mechanically strong to withstand the applied pressure difference.

The asymmetric macropore structure of petrified hollow fiber membranes makes them promising for pressure-driven filtration (e.g., ultrafiltration). Porous oxide ultrafiltration membranes are traditionally based on sintered alumina supports.<sup>26</sup> Because of the difficulty to precisely control pore sizes in sintered alumina, a secondary slip or sol-gel coating layer<sup>27</sup> must be applied to reject sub-100 nm macromolecular solutes. As petrified hollow fiber membranes reproduce the asymmetric macropore structure of their polymer hollow fiber templates, they can provide attractive rejection of macromolecular solutes without slip or sol-gel coating. We carried out cross-flow filtration measurements<sup>28</sup> on the petrified hollow fiber membranes using a 0.5 g/L bovine serum albumin (BSA, molecular weight ~66 kDa) solution at 1 bar TMP. Following 3 h filtration, the petrified hollow fiber membranes showed outstanding BSA rejection above 99% (Figure 3c). It should be noted that BSA molecules (~11 nm) are much smaller than the top surface pore diameter (Figure 1c) of the petrified hollow fiber membranes. The high BSA rejection was

likely facilitated by formation of a fouling layer, which is indicated by the water flux decline over time.

In conclusion, for the first time, we show that petrified hollow fiber membranes with hierarchical pores can be made at a moderate temperature of 600 °C. To our best knowledge, this is the lowest fabrication temperature reported for porous oxide hollow fiber membranes. Like the geometry and cell structure of organic wood are reproduced in petrified wood, the geometry and macropore structure of organic polymer hollow fiber templates are reproduced in petrified hollow fiber membranes. Albeit inorganic, these petrified hollow fiber membranes have asymmetric pore structure closely resembling polymer hollow fiber membranes.<sup>29</sup> The asymmetric pore structure allows petrified hollow fiber membranes to provide high rejection of macromolecular solutes without a secondary coating layer. The results of this work open the door to a new paradigm of porous oxide hollow fiber membranes widely useful for filtration and separations. More broadly, the novel petrification method allows simple and catalyst-free fabrication of hierarchically porous oxides with controlled geometry and simultaneous high surface area and large pore volume.

## ASSOCIATED CONTENT

## **Solution** Supporting Information

The Supporting Information is available free of charge at https://pubs.acs.org/doi/10.1021/acsmaterialslett.2c00063.

Experimental procedures regarding fabrication of polymer hollow fiber templates, formation of petrified hollow fiber membranes, membrane permeation and filtration measurements, and characterizations (energy dispersive X-ray analysis, thermogravimetric analysis, powder X-ray diffraction,  $N_2$  and Ar physisorption, water vapor adsorption); supplementary text; supplementary figures and tables (PDF)

## AUTHOR INFORMATION

## **Corresponding Author**

Chen Zhang — Department of Chemical and Biomolecular Engineering, University of Maryland, College Park, Maryland 20742, United States; orcid.org/0000-0002-0071-2898; Email: czhang71@umd.edu

# **Authors**

Lu Liu – Department of Chemical and Biomolecular Engineering, University of Maryland, College Park, Maryland 20742, United States

Ching-En Ku — Department of Chemical and Biomolecular Engineering, University of Maryland, College Park, Maryland 20742, United States

Complete contact information is available at: https://pubs.acs.org/10.1021/acsmaterialslett.2c00063

### Funding

This work was supported by the National Science Foundation under award CBET-2044794.

### Notes

The authors declare the following competing financial interest(s): The authors are inventors of a U.S. patent application submitted by the University of Maryland.

## ACKNOWLEDGMENTS

The authors thank D. Liu for kindly providing access to TGA and UV—vis instruments and G. Iyer for contributions to fabricating the polymer hollow fiber templates. C.Z. thanks faculty summer support from the Minta Martin Award. L.L. is grateful for the Hulka Energy Research Fellowship provided by the Maryland Energy Innovation Institute.

### REFERENCES

- (1) Xu, J.; Chang, C.-Y.; Gao, C. Performance of a ceramic ultrafiltration membrane system in pretreatment to seawater desalination. *Sep. Purif. Technol.* **2010**, 75, 165–173.
- (2) Kim, D.; Jeon, M. Y.; Stottrup, B. L.; Tsapatsis, M. para-Xylene Ultra-selective Zeolite MFI Membranes Fabricated from Nanosheet Monolayers at the Air-Water Interface. *Angew. Chem., Int. Ed.* **2018**, 57, 480-485.
- (3) DeWitt, S. J. A.; Sinha, A.; Kalyanaraman, J.; Zhang, F.; Realff, M. J.; Lively, R. P. Critical Comparison of Structured Contactors for Adsorption-Based Gas Separations. *Annu. Rev. Chem. Biomol. Eng.* **2018**, *9*, 129–152.
- (4) Zydney, A. L. New developments in membranes for bioprocessing A review. J. Membr. Sci. 2021, 620, 118804.
- (5) Mirfendereski, S. M.; Lin, J. Y. S. High-performance MFI zeolite hollow fiber membranes synthesized by double-layer seeding with variable temperature secondary growth. *J. Membr. Sci.* **2021**, *618*, 118573.
- (6) Zhou, R.; Ping, E. W.; Funke, H. H.; Falconer, J. L.; Noble, R. D. Improving SAPO-34 membrane synthesis. *J. Membr. Sci.* **2013**, 444, 384–393.
- (7) Liang, F.; Jiang, H.; Schiestel, T.; Caro, J. High-Purity Oxygen Production from Air Using Perovskite Hollow Fiber Membranes. *Ind. Eng. Chem. Res.* **2010**, *49*, 9377–9384.
- (8) Xu, L.; Zhang, C.; Rungta, M.; Qiu, W.; Liu, J.; Koros, W. J. Formation of defect-free 6FDA-DAM asymmetric hollow fiber membranes for gas separations. *J. Membr. Sci.* **2014**, 459, 223–232.
- (9) Tan, X.; Li, K. Inorganic hollow fibre membranes in catalytic processing. *Curr. Opin. Chem. Eng.* **2011**, *1*, 69–76.
- (10) Sakbodin, M.; Wu, Y.; Oh, S. C.; Wachsman, E. D.; Liu, D. Hydrogen-Permeable Tubular Membrane Reactor: Promoting Conversion and Product Selectivity for Non-Oxidative Activation of Methane over an Fe©SiO2 Catalyst. *Angew. Chem., Int. Ed.* **2016**, *55*, 16149–16152.
- (11) Hassan, M. H.; Douglas Way, J.; Thoen, P. M.; Dillon, A. C. Single component and mixed gas transport in a silica hollow fiber membrane. *J. Membr. Sci.* **1995**, *104*, 27–42.
- (12) Kwon, Y. H.; Min, B.; Yang, S.; Koh, D.-Y.; Bhave, R. R.; Nair, S. Ion-Exchanged SAPO-34 Membranes for Krypton—Xenon Separation: Control of Permeation Properties and Fabrication of Hollow Fiber Membranes. ACS Appl. Mater. Interfaces 2018, 10, 6361–6368.
- (13) Li, W.; Liu, J.; Zhao, D. Mesoporous materials for energy conversion and storage devices. *Nat. Rev. Mater.* **2016**, *1*, 16023.
- (14) Szczęśniak, B.; Choma, J.; Jaroniec, M. Major advances in the development of ordered mesoporous materials. *Chem. Commun.* **2020**, *56*, 7836–7848.
- (15) Petkovich, N. D.; Stein, A. Controlling macro- and mesostructures with hierarchical porosity through combined hard and soft templating. *Chem. Soc. Rev.* **2013**, *42*, 3721–3739.
- (16) Ren, Y.; Ma, Z.; Bruce, P. G. Ordered mesoporous metal oxides: synthesis and applications. *Chem. Soc. Rev.* **2012**, *41*, 4909–4927.
- (17) Sigleo, A. C. Organic geochemistry of silicified wood, Petrified Forest National Park, Arizona. *Geochim. Cosmochim. Acta* 1978, 42, 1397–1405.
- (18) Zhang, C.; Kumar, R.; Koros, W. J. Ultra-thin skin carbon hollow fiber membranes for sustainable molecular separations. *AIChE J.* **2019**, *65*, e16611.

- (19) Bhuwania, N.; Labreche, Y.; Achoundong, C. S. K.; Baltazar, J.; Burgess, S. K.; Karwa, S.; Xu, L.; Henderson, C. L.; Williams, P. J.; Koros, W. J. Engineering substructure morphology of asymmetric carbon molecular sieve hollow fiber membranes. *Carbon* **2014**, *76*, 417–434.
- (20) Leofanti, G.; Padovan, M.; Tozzola, G.; Venturelli, B. Surface area and pore texture of catalysts. *Catal. Today* **1998**, *41*, 207–219.
- (21) Diniz da Costa, J. C.; Lu, G. Q.; Rudolph, V.; Lin, Y. S. Novel molecular sieve silica (MSS) membranes: characterisation and permeation of single-step and two-step sol-gel membranes. *J. Membr. Sci.* **2002**, *198*, 9–21.
- (22) Siddique, H.; Rundquist, E.; Bhole, Y.; Peeva, L. G.; Livingston, A. G. Mixed matrix membranes for organic solvent nanofiltration. *J. Membr. Sci.* **2014**, 452, 354–366.
- (23) Dose, M. E.; Zhang, K.; Thompson, J. A.; Leisen, J.; Chance, R. R.; Koros, W. J.; McCool, B. A.; Lively, R. P. Effect of Crystal Size on Framework Defects and Water Uptake in Fluoride Mediated Silicalite-1. *Chem. Mater.* **2014**, *26*, 4368–4376.
- (24) Adams, J. S.; Itta, A. K.; Zhang, C.; Wenz, G. B.; Sanyal, O.; Koros, W. J. New insights into structural evolution in carbon molecular sieve membranes during pyrolysis. *Carbon* **2019**, *141*, 238–246.
- (25) Silva, L. L. O.; Vasconcelos, D. C. L.; Nunes, E. H. M.; Caldeira, L.; Costa, V. C.; Musse, A. P.; Hatimondi, S. A.; Nascimento, J. F.; Grava, W.; Vasconcelos, W. L. Processing, structural characterization and performance of alumina supports used in ceramic membranes. *Ceram. Int.* **2012**, *38*, 1943–1949.
- (26) Ding, X.; Fan, Y.; Xu, N. A new route for the fabrication of TiO2 ultrafiltration membranes with suspension derived from a wet chemical synthesis. *J. Membr. Sci.* **2006**, *270*, 179–186.
- (27) Baker, R. W. Membrane Technology and Applications. John Wiley and Sons Ltd: 2012.
- (28) Kazemi, A. S.; Patterson, B.; LaRue, R. J.; Papangelakis, P.; Yoo, S. M.; Ghosh, R.; Latulippe, D. R. Microscale parallel-structured, cross-flow filtration system for evaluation and optimization of the filtration performance of hollow-fiber membranes. *Sep. Purif. Technol.* **2019**, 215, 299–307.
- (29) Clausi, D. T.; Koros, W. J. Formation of defect-free polyimide hollow fiber membranes for gas separations. *J. Membr. Sci.* **2000**, *167*, 79–89.